Available online at www.sciencedirect.com
SCIENCE DIRECT®
Journal of Organometallic Chemistry 666 (2003) 75–85
Journal of Organometallic Chemistry
www.elsevier.com/locate/jorganchem

Ligand-mediated metal–metal interactions and localized versus delocalized mixed-valence cation states of biferrocene and bis(μ-fulvalenediyl)diiron characterized in the gas phase by valence photoelectron spectroscopy

Dennis L. Lichtenberger *, Hua-Jun Fan, Nadine E. Gruhn

Department of Chemistry, Center for Gas-Phase Electron Spectroscopy, The University of Arizona, Tucson, AZ 85721-0041, USA

Received 8 August 2002

Abstract

Gas-phase photoelectron spectroscopy is used to investigate metal–metal interactions and the mixed-valence positive ion states of biferrocene and bis(μ-fulvalenediyl)diiron. The spectra of phenylferrocene and 1,1′-diphenylferrocene are used to show that, in comparison to ferrocene, the extension of the ligand π system and the reduced ligand symmetry do not have an appreciable effect on the band profile of the metal-based ionizations. In contrast, the initial ionization bands of both bimetallic molecules, which derive from the metal-based $^2E_{2g}$ ionizations of ferrocene, are spread over a wide energy range, indicating delocalization across the two metal halves of the molecule and formal oxidation states of $+2^1/_2$ for each metal atom in these cation states. The broadening and splitting of this ionization band for bis(μ-fulvalenediyl)diiron is twice that observed for biferrocene, consistent with a through-bond ligand-mediated mechanism of interaction. Ionizations of the bimetallic molecules that derive from the metal-based $^2A_{1g}$ ionizations of ferrocene occur in a single narrow band, indicating that both through-space and through-ligand interactions are not appreciable for the d_{z^2}-based orbitals. The difference between the metal–metal interactions in these positive ion states follows from the different overlap and energy match of the metal orbitals with fulvalendiyl orbitals of the appropriate symmetry. Most important to the metal–metal interaction in the ground ion state are empty fulvalendiyl orbitals with two nodes perpendicular to the C_5 planes and *gerade* and *ungerade* symmetries with respect to the inversion centers of the molecules. In the gas phase, both species are found to be strongly interacting, delocalized mixed-valence compounds in their ground ion states.

Keywords: Photoelectron spectroscopy; Mixed-valence; Fulvalendiyl; Biferrocene

1. Introduction

Evaluation of electron transfer processes has gained much attention due to their importance in biological systems [1], and their potential application in molecular electronics and molecular sensors [2]. Many studies of electronic communication between two sites in a system have focused on bimetallic molecules with metal centers of mixed valency [3,4], in particular molecules that contain a delocalized bridging ligand such as 4,4′-bipyridine [5] or polyynes [6], and bi- sandwich molecules of biphenyl, and fulvalenediyl [2,7–9]. Molecular and supramolecular [10] systems incorporating metallocenes and most notably ferrocene have been extensively studied. In particular, two molecules that can be considered classical test cases for evaluating electronic communication are biferrocene, $Fv(FeCp)_2$, where Cp is cyclopentadienyl (η^5-$C_5H_5^-$), and *bis*(μ-fulvalenediyl)diiron, Fv_2Fe_2, where Fv is fulvalenediyl [11] (μ-η^5:η^5-$C_{10}H_8^{2-}$).

These two molecules are useful models not only because they have discrete electron transfer properties that can easily be evaluated by a number of spectroscopic methods [12–15], but also because they can provide insight into the factors of electron transfer by comparing two molecules that have similar metal centers

* Corresponding author
E-mail address: dlichten@u.arizona.edu (D.L. Lichtenberger).

0022-328X/02/$ - see front matter © 2002 Published by Elsevier Science B.V.
PII: S0022-328X(02)02035-1

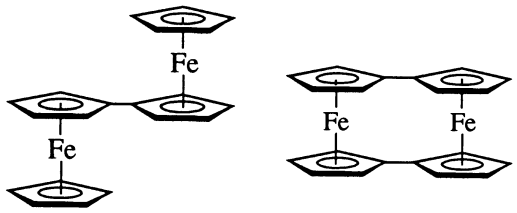

$Fv(FeCp)_2$ Fe_2Fv_2

but a different overall molecular geometry with much different metal–metal distances.

Mössbauer spectroscopy [16] has shown that both the neutral species Fv_2Fe_2 and $Fv(FeCp)_2$ and the dioxidized species $[Fv_2Fe_2]^{2+}$ and $[Fv(FeCp)_2]^{2+}$ have equivalent iron centers. In contrast, while the Mössbauer spectrum of $[Fv_2Fe_2]^{+}$ was shown to exhibit two equivalent iron centers even at 77 K, the spectrum of $[Fv(FeCp)_2]^{+}$ at this temperature resembles a combination of the spectra of ferrocene and ferrocenium indicating two iron centers with different charges. Solid-phase X-ray photoelectron spectroscopy also shows the equivalence of the two iron atoms in $[Fv_2Fe_2]^{+}$ [17]. From these previous studies, $[Fv(FeCp)_2]^{+}$ has been considered a class II species according to the classification system of Robin and Day for mixed-valence molecules [18], indicating that some properties of distinct, localized Fe^{II}/Fe^{III} components are discernible under certain conditions, while $[Fv_2Fe_2]^{+}$ has been considered a class III species, indicating strong interaction and delocalization of the unpaired electron between the two metal centers corresponding to oxidation states of 2.5 for each metal atom [12–15].

Delocalization of the unpaired electron in the mixed valence state implies electronic connection between the two metals. The pathway for such connection between the two metal centers in these molecules is still not completely understood. While a through-space interaction between the two metal centers of $Fv(FeCp)_2$ would be small considering the *transoid* geometry of the molecule, Hillman and Kvick [19] have proposed that a direct through-space iron–iron interaction is present in $[Fv_2Fe_2]^{+}[PF_6]^{-}$ based on crystallographic data of the cation species. Furthermore, Böhm [20] has reported He I photoelectron spectra for Fv_2Fe_2 and $Fv(FeCp)_2$. The photoelectron spectra were assigned based on computational results from semiempirical INDO molecular orbital calculations [21]. Based on these computational results, Böhm concluded that no appreciable through-space interaction occurs between the metal centers of these molecules, that hole exchange for both of these molecules is too fast to couple with a vibrational mode in the time-frame of photoelectron spectroscopy, and therefore that these molecules actually contain two *inequivalent* iron sites in trapped valences. However, due to the limitations of the computational methods and the poor resolution of the photoelectron spectra, these issues deserve closer examination.

In this study, the gas-phase He I and He II photoelectron spectra of Fv_2Fe_2 and $Fv(FeCp)_2$ are reported and used to analyze the metal–metal communication present in the cation states formed by photoionization. The data reported here are of much higher precision and signal-to-noise than the He I data previously reported [21] and analysis leads to a different assignment of the lowest energy cation state than the previous study. Important features of the ionization profiles that give insight to the mixed-valence states are revealed. The photoelectron spectra of phenylferrocene (FcPh) and 1,1′-diphenylferrocene ($FcPh_2$) are also reported and used to evaluate the effect of the extended π interaction in the ligand and lowered symmetry of the molecules on the ion states.

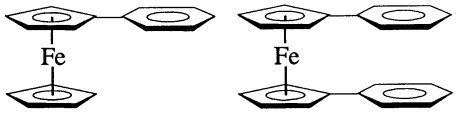

FcPh $FcPh_2$

These photoelectron experiments give a measure of the metal–metal communication in the gas phase for comparison with the results of other spectroscopic techniques that have studied these species in solution or the solid state. The fast time scale of the photoelectron experiment precludes any time averaging of geometries or localized states. In addition, the photoelectron technique has the advantage of providing information on the metal–metal interaction for not only the ground state of the ion, but also for excited electronic states of the ion. Evaluation of this spectroscopic information gives insight into the factors that control electronic communication between two or more metals in molecular and supramolecular systems.

2. Experimental

2.1. Preparation of compounds

The compounds Fv_2Fe_2 and $Fv(FeCp)_2$ were synthesized and characterized using published methods [17,22]. The compounds FcPh and $FcPh_2$ were prepared and characterized by slight modifications of literature procedures [23–25], with the following details for the example of FcPh. In the presence of $ZnCl_2$ (21.36 mmol) and $PdCl_2(PPh_3)_2$ (0.6 mmol), 18 mmol of ferrocene in THF was reacted with 20 mmol of ^{t}BuLi

in C_5H_{12}. The mixture was then reacted with 18 mmol of bromobenzene and quenched with 12 ml 2 M HCl thereafter. The final product was extracted and sublimed in vacuum. The crystal was obtained from C_3H_8O by slow evaporation of solvent and the structure was solved using direct methods followed by Fourier synthesis in the Molecular Structure Laboratory of the Department of Chemistry, University of Arizona [26]. ^{1}H-NMR and mass spectra were used to verify the compounds.

2.2. Data collection

Photoelectron spectra were collected using an instrument that features a 36 cm hemispherical analyzer (McPherson) and custom designed sample cells, excitation source, and detection and control electronics that have been described elsewhere [27]. The argon $^2P_{3/2}$ ionization peak at 15.759 eV was used as an internal calibration lock of the absolute ionization energy. The difference between the argon $^2P_{3/2}$ ionization peak and the methyl iodide $^2E_{1/2}$ at 9.538 eV was used to calibrate the ionization energy scale. Both He I and He II valence spectra were collected for all four molecules. During data collection, the instrument resolution (FWHM of the Ar $^2P_{3/2}$ peak) was 16–18 meV for HeI and 20 meV for He II. The sublimation temperatures of compounds were: Fv_2Fe_2 (180 °C), $Fv(FeCp)_2$ (130 °C), FcPh (80 °C), and $FcPh_2$ (120 °C) (monitored by a 'K' type thermocouple attached to the cell).

2.3. Data analysis

All of the He II spectra were corrected for the He II β source excitation (48.4 eV, 12% intensity of He II α source). The data are represented analytically in terms of asymmetric Gaussian peaks, which are defined by the position, half widths on the high and low binding energy side, and the amplitude. The vertical dashed lines in the figures of the spectra are the actual data points with the length of the line representing the variance of each data point. The number of peaks used for the analytical representation is based solely on the profile of a given band. This procedure has been described elsewhere in more detail [28]. The uncertainty in the relative band areas is on the order of 5% for overlapping peaks and less than 2% for well separated ionization bands. The confidence of the peak positions was typically ±0.02 eV. Parameters for overlapping bands may be interdependent and less certain.

2.4. Theoretical details

The geometries of neutral and cationic states were optimized using the Amsterdam Density Functional package, version 2.3.0 [29–32] at the local density approximation ($\alpha = 0.7$) level. The calculated structures compare well with the reported X-ray diffraction structures [17,33]. Fenske-Hall calculations [34] using the structures from the ADF calculations were carried out for the purpose of comparing individual orbital interactions. The atomic basis functions for the Fenske-Hall calculations were generated using the method of Bursten et al. [35]. Contracted double-zeta functions were used for the Fe valence d atomic orbitals and for the C 2p atomic orbitals. Basis functions for the metal atoms were derived for the +1 oxidation state. Ground state atomic configurations were used for the basis functions of all other atoms. Visualizations of the molecular orbital isosurfaces were produced using VTK [36] developed in this laboratory [37].

3. Results

3.1. General ionization features

General assignments of the ionizations will be presented in this section with more detailed analysis that gives insight to the metal–metal communication reserved for the Section 4. The He I valence photoelectron spectra of the compounds studied here are shown in Fig. 1 with the spectrum of ferrocene shown in Fig. 1A for comparison. In each of these spectra the energy region above about 10.5 eV contains ionizations arising from C–C and C–H σ-bonding orbitals, as well as the lowest energy, completely symmetric π-based ionizations of Cp and/or Fv. Due to a large degree of overlap among these ionizations, this region does not provide much interpretable information and only the ionization bands located from 5.5 to 10.5 eV will be examined closely. The assignments for the ionizations in this low energy region along with the analytical representations of bands **1**, **2**, and **3′** are listed in Table 1. Several overlapping ionizations are discernable in region **3**, but

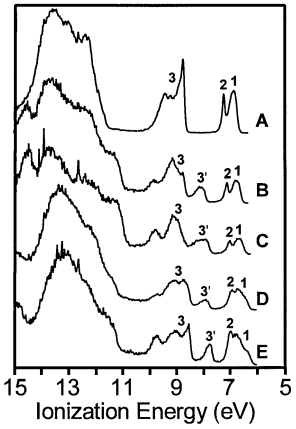

Fig. 1. Gas-phase valence photoelectron spectra of: (A) ferrocene; (B) phenylferrocene; (C) 1,1′-diphenylferrocene; (D) biferrocene ($Fv(FeCp)_2$), and (E) bis(μ-fulvalenediyl)diiron (Fv_2Fe_2).

the specific energies and contours of individual ionizations in this region are not important to this study. For sake of conciseness, only the energy range and total relative ionization area in this region are listed in Table 1. The assignments of the ionizations **1**, **2**, and **3′** follow from comparison of the band positions and shapes with those of the ferrocene spectrum, by comparisons within the series, and by comparisons of He I and He II ionization intensities (vide infra). The ionizations generally reflect the combination of two ferrocene molecules. The ionization peaks labeled **1**, **2**, and **3** for $Fv(FeCp)_2$ and Fv_2Fe_2 represent twice as many ionizations as the peaks labeled **1**, **2**, and **3** for ferrocene, because each half of the bimetallic molecule fragment contributes one corresponding ferrocene-type ionization. For all these molecules the ionization bands **1** and **2** are predominantly metal d-orbital based and ionization bands **3′** and **3** are predominantly ligand π-orbital based. These assignments reflect the primary orbital character associated with the ionizations, but as will be shown significant mixing of metal and ligand character is often present. Important observations are that the ionization envelopes of bands **1** of Fv_2Fe_2 and $Fv(FeCp)_2$ are rather different from those of ferrocene, and that the ligand-based ionizations have been spread over a broader energy region than for ferrocene.

3.2. Ferrocene ionizations

A short review of the assignments of the ionization bands of ferrocene is helpful before the assignments of the ionizations of the molecules studied here are considered in greater detail, with further details available elsewhere [38–40]. D_{5d} symmetry will be utilized for labeling the ion states. The low-energy ionizations of ferrocene (Fig. 1A) are divided into three types. The ionization labeled **1** is assigned to the $^2E_{2g}$ ion state. This ion state corresponds to removal of an electron from the e_{2g} orbital, which is composed primarily of the metal d_{xy} and $d_{x^2-y^2}$ orbitals but also has significant ligand π character due to mixing with the unoccupied Cp_2 e^*_{2g} orbital. Ionization band **2** corresponds to the $^2A_{1g}$ ion state, or removal of an electron from the a_{1g} orbital that is almost completely metal d_{z^2}-based due to very poor overlap and energy matching with the filled ligand π-based orbital of a_{1g} symmetry. A second low intensity Gaussian is needed to properly model the shape of ionization **2** due to the presence of a short vibrational

Table 1
Analytical representations of the valence ionizations 1, 2, and 3′ and the energy range and collected relative areas of ionizations in region 3

Band	Position (eV)	Half width		Relative area		Label
		High	Low	He I	He II	
Ferrocene						
1	6.86	0.46	0.21	3.50	2.94	$^2E_{2g}$
2	7.25	0.13	0.09	1	1	$^2A_{1g}$
3	8.75–9.84			9.94	4.11	$^2E_{1g}$, $^2E_{1u}$
FcPh						
1	6.72	0.48	0.25	3.23	2.94	d_{xy}, $d_{x^2-y^2}$
2	7.10	0.17	0.11	1	1	d_{z^2}
3′	8.02	0.66	0.21	2.64	1.5	Cp, Ph
3	8.73–10.05			15.52	5.97	Cp, Ph
$FcPh_2$						
1	6.67	0.50	0.28	3.33	3.13	d_{xy}, $d_{x^2-y^2}$
2	7.05	0.15	0.12	1	1	d_{z^2}
3′	7.92	0.46	0.24	6.23	2.94	Cp, Ph
	8.25	0.73	0.25			
3	9.00–10.41			21.37	7.50	Cp, Ph
$Fv(FeCp)_2$						
1	6.50, 6.73	0.39	0.26	2.61	2.26	d_{xy}, $d_{x^2-y^2}$
2	7.00	0.24	0.21	1	1	d_{z^2}
3′	7.90	0.65	0.18	0.97	0.48	$Fv(a_g)$
3	8.6–9.75			9.57	2.80	Fv, Cp
Fv_2Fe_2						
1	6.36, 6.62, 6.83	0.36	0.27	3.63	2.61	d_{xy}, $d_{x^2-y^2}$
2	7.00	0.22	0.15	1	1	d_{z^2}
3′	7.72	0.41	0.14	1.09	0.37	$Fv(b_{3u})$
3	8.53–9.73			7.84	3.37	Fv

progression. Ionization band **3** is attributed to the $^2E_{1u}$ and $^2E_{1g}$ ion states, which correspond to ionizations from the predominantly Cp-based e_{1u} and e_{1g} orbitals. These Cp-based orbitals are the symmetry combinations of the one-node Cp π e_1'' orbitals. The lower ionization energy portion of band **3** is associated with the $^2E_{1u}$ ion state while the $^2E_{1g}$ ion state occurs at slightly higher ionization energy. The e_{1u} orbital is almost completely ligand based because the only metal orbitals that can interact with this orbital by symmetry are the high-energy occupied metal 3p orbitals and the virtual metal 4p orbitals. The e_{1g} orbital in contrast has extensive mixing with the unfilled metal orbitals of e_{1g} symmetry (d_{xz}/d_{yz}), and this bonding interaction results in the Cp-based e_{1g} orbital being stabilized compared to the e_{1u} orbital. This interaction also accounts for the broadening of the e_{1g} ionization relative to the e_{1u} ionization. These assignments are consistent with all photoelectron spectroscopic studies that have been performed on ferrocene, including variable photon energy studies and evaluation of the effects of substitution of different groups on the cyclopentadienyl ligands [41]. The electronic structure of the ferrocenium cation has also been investigated by EPR studies, and agrees with the photoelectron spectroscopy in that the $^2E_{2g}$ is the ground state configuration of the cation, and that the $^2A_{1g}$ state is an excited state of the cation [42]. The relative energy of these ion states reflects the large amount of relaxation and correlation effects that are often encountered for organometallic molecules, and has been discussed in greater detail elsewhere [40]. Two points are important for later assignment and discussion of the metal-based ionizations of the bimetallic molecules: the first is the sharpness of the predominantly metal d_{z^2} orbital ionization (**2**), which indicates the non-bonding nature of this orbital; and second is the relatively intensity of bands **1** and **2** at their maximum amplitude. As will be shown, the trends observed in the metal-based ionizations of Fv_2Fe_2 and $Fv(FeCp)_2$ indicate that the relative ordering of the ion states for these molecules that are descended from the $^2E_{2g}$ and $^2A_{1g}$ ion states remains the same as for ferrocene, in contrast to the assignment originally suggested by Böhm [21].

An indication of the atomic character in ionization bands can be obtained by examining the relative intensity changes of ionization bands between He I and He II spectra and by assuming that atomic cross sections are additive in a molecule. The relative intensity of an ionization will increase in a He II spectrum compared to a He I spectrum if the corresponding orbital contains iron character as compared to an ionization from an orbital of primarily carbon character [41]. As an example, the He I and He II spectra of the lower valence region of $Fv(FeCp)_2$ are shown in Fig. 2

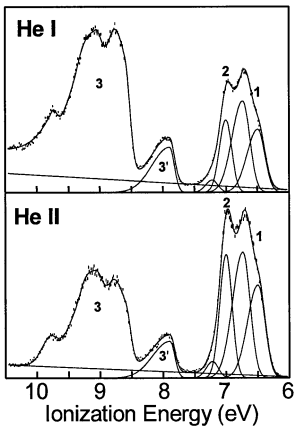

Fig. 2. He I and He II spectra of the low valence ionization energy region of biferrocene ($Fv(FeCp)_2$).

and the relative band areas for all the molecules studied here are listed in Table 1.

3.3. Phenylferrocene (FcPh) and 1,1′-diphenylferrocene ($FcPh_2$)

The electronic interactions of the π orbitals between the phenyl ring and the Cp ring in FcPh and $FcPh_2$ can be used to model the electronic interactions between the two rings in the Fv ligand and to examine the effect of ligand π delocalization and lower symmetry on the electronic structure of substituted ferrocenes. The crystal structure of phenylferrocene [26] and other π-conjugated ligands on ferrocene [43,44] show that the angle between the plane containing five carbon atoms in Cp and the plane containing six carbon atoms in phenyl is around 10°, with the small deviation from planarity most likely influenced by packing forces in the solid state.

Close-up spectra of phenylferrocene and 1,1′-diphenylferrocene are shown in Fig. 3 along with that of ferrocene for comparison. The similarity of the spectra

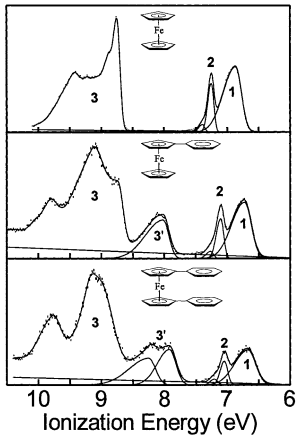

Fig. 3. The low valence ionization energy region of ferrocene, phenylferrocene, and 1,1′-diphenylferrocene.

of the phenyl-substituted molecules to that of unsubstituted ferrocene is apparent. The three spectra each have peaks labeled **1** and **2** that are associated with the metal d ionizations and peaks labeled **3** associated with the ligand π ionizations. The metal ionizations of both phenyl-substituted molecules are shifted slightly to lower ionization energy from that of ferrocene due to the greater electron donor ability of phenyl compared with hydrogen on the Cp ring. With the increasing electron flow to the metal center, the metal ionizations are destabilized about 0.16 eV for FcPh and 0.21 eV for $FcPh_2$. However, compared with ferrocene the relative energies, widths, and relative intensities of band **1** and **2** for both FcPh and $FcPh_2$ have not changed.

In contrast to the general similarity of the metal-based ionizations of FcPh and $FcPh_2$ to those of ferrocene, significant differences in the band profiles of the ligand-based ionizations labeled **3** are observed. One primary difference is that the molecules with phenyl-substituted cyclopentadienyl rings have additional ligand-based ionizations labeled **3′** located near 8 eV that have no counterpart in the ferrocene spectrum. For FcPh and $FcPh_2$ the ionizations labeled **3** and **3′** are derived from the e_{1g} and e_{1u} orbitals of ferrocene and the e_{1g} orbitals of benzene. The profile change in the Cp-based ionization region compared to ferrocene reflects the interactions between the Cp- and Ph-based orbitals. Each degenerate set of Cp- and Ph-fragment orbitals will have one component that has a node across the Cp–Ph bond and therefore almost no net overlap effect. The Cp- and Ph-fragment based π orbitals that do have character on the Cp–Ph bonded carbons will form strongly bonding and antibonding combinations. As shown below, the highest occupied orbital of the phenylcyclopentadienyl fragment is an anti-symmetric combination across the bridging carbons. Similarly, band **3′** of FcPh is due to a strongly destabilizing filled-filled interaction of one component of the Cp-based e_{1u} orbital of ferrocene with a π orbital of the phenyl substituent.

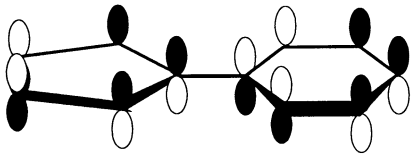

Band **3′** of $FcPh_2$ consists of two ionizations that arise from two combinations of the phenylcyclopentadienyl orbital shown above. The combined area of band **3′** for $FcPh_2$ is twice that of band **3′** for FcPh, as expected for the two ionizations, and the profile shows a splitting of 0.34 eV. With the traditional definition of the z-axis pointing from the metal center to the Cp centroid, the splitting is dependent on the rotational orientation of the two CpPh rings around the z-axis. If the CpPh fragments are rotated such that the phenyl rings are eclipsed (0° rotation angle around the z-axis) or opposite each other (180° rotation around the z-axis), then one of the combinations contributing to **3′** has the symmetry to be stabilized by interaction with a metal d orbital, and a splitting between the two ionizations is expected. If the CpPh fragments are rotated to a 90° angle orientation, the Cp nodes are orthogonal and there should be little splitting because neither combination has the symmetry to interact with the metal. Fenske-Hall calculations predict that the splitting of band **3′** would be 0.63 eV at a 0° rotation angle, 0.07 eV at a 90° rotation angle, and 1.14 eV at a 180° rotation angle. The observed splitting indicates that the preferred rotation of the CpPh fragments is not 90°, but the exact angle is uncertain.

3.4. Biferrocene ($Fv(FeCp)_2$)

For sake of comparison the He I close-up spectra of ferrocene, $Fv(FeCp)_2$, and Fv_2Fe_2 are shown in Fig. 4. The metal-based ionizations of $Fv(FeCp)_2$ and ferrocene are generally similar, indicating that the order of the primarily $d_{x^2-y^2}/d_{xy}$ and d_{z^2} ionizations is still the same for $Fv(FeCp)_2$ as for ferrocene. The information from the He II spectrum is also consistent with this assignment, showing that the intensity of band **1** decreases compared to band **2** due to the significant ligand character present in the primarily $d_{x^2-y^2}/d_{xy}$-based orbitals. Band **1** of the bimetallic molecules contains four ionizations derived from the two $^2E_{2g}$ ionizations of the two ferrocene-like halves of the molecule. Without communication between these two halves the ionizations would have the same contour as that of ferrocene and the phenylferrocenes just discussed. As can be seen, the contour of band **1** in the spectrum of $Fv(FeCp)_2$ has changed compared to the contour of the corresponding bands of ferrocene and the phenyl-substituted ferrocenes. At least two Gaussians are needed to model the appearance of band **1** for $Fv(FeCp)_2$. The exact splitting

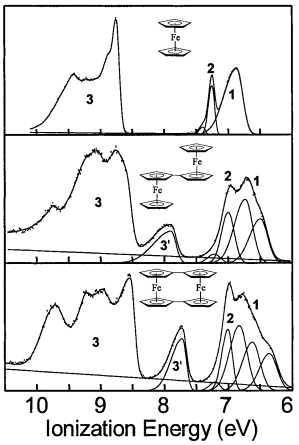

Fig. 4. The low valence ionization energy region of ferrocene, biferrocene ($Fv(FeCp)_2$) and bis(μ-fulvalenediyl)diiron (Fv_2Fe_2).

within band **1** is difficult to determine due to the overlap with band **2**, but the change in band profile from the monometallic to the bimetallic complex is clear. This splitting is due to the electronic interactions between the two halves of the molecule, and will be further addressed in Section 4. In contrast, no apparent splitting is revealed for band **2**, which contains two ionizations derived from the $^2A_{1g}$ ionizations of the ferrocene-like halves of the molecule. For these ionizations there is little apparent communication between the two metal centers. Furthermore, the relatively narrow width of this band indicates that there is little geometry change of the molecule to this ion state. Thus the d_{z^2} orbitals remain primarily non-interacting.

Ionization bands **3′** and **3** are assigned to ionizations from orbitals that are primarily cyclopentadienyl and fulvalenediyl π in character. A detailed illustration of the Fv ligand orbital construction can be found elsewhere [45]. The ionization **3′** of $Fv(FeCp)_2$ has previously been assigned to the fulvalenediyl orbital of a_g symmetry [21]. The nodal properties of this orbital are illustrated below. The nodal properties of this orbital show that it has an antisymmetric interaction across the linking carbon atoms and negligible interaction with the metal d-orbitals. This orbital can be thought of as arising from the anti-bonding combination of two ferrocene e_{1u} Cp-based orbitals.

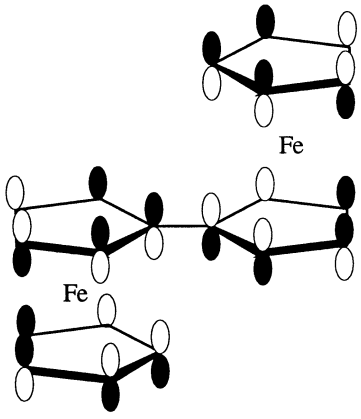

3.5. Bis(μ-fulvalenediyl)diiron (Fv_2Fe_2)

As shown in Fig. 4 the shape of the metal-based ionization band **1** of Fv_2Fe_2 has greatly changed from that of ferrocene and even more so now than observed for $Fv(FeCp)_2$. Three Gaussian peaks are needed to model the shape of band **1** in Fv_2Fe_2 in order to obtain a satisfactory account of the contour. Contrary to what is observed in the spectra of ferrocene and $Fv(FeCp)_2$, peak **2** of Fv_2Fe_2 now has greater intensity at its maximum than peak **1** due to further energy spreading of band **1** in Fv_2Fe_2. The width of peak **2** is now more clearly observed than for $Fv(FeCp)_2$, and it is clear that peak **2** retains its narrow width.

The ionization **3′** of Fv_2Fe_2 has previously been assigned to the fulvalenediyl-based orbital of b_{3u} symmetry [21]. The nodal properties of this orbital are similar to those of band **3′** in $Fv(FeCp)_2$ shown previously, but with an additional anti-symmetric combination across the bridging carbon–carbon bond of the second fulvalenediyl ligand (see diagram a below). Similar to the corresponding orbital of $Fv(FeCp)_2$, this orbital again has almost no interaction with the metal d-orbitals due to its nodal properties. Whereas the spectrum of $FcPh_2$ had two ionizations in this energy region that were split by 0.33 eV, the spectrum of Fv_2Fe_2 has only one ionization well separated from the other ligand ionizations as indicated by the ionization band profile and the integrated cross section listed in Table 1. The companion combination orbital to **3′** has nodal properties as shown in diagram b below. This orbital is similarly antibonding across the carbon atoms that link the rings, but it has the correct symmetry to donate and bond into the empty metal d orbitals. As a consequence, it is stabilized at least 0.8 eV in ionization energy in comparison to **3′** and is located under the ionization band labeled **3**. This is a slightly greater separation than the splitting of the Cp e_{1u} and e_{1g} ionizations of ferrocene (0.69 eV) and almost double the splitting of band **3′** presented in $FcPh_2$, presumably due to the exactly 0° alignment of the two fulvalenediyl ligands and the resultant better donor ability of this fulvalenediyl orbital to the unfilled metal d orbitals.

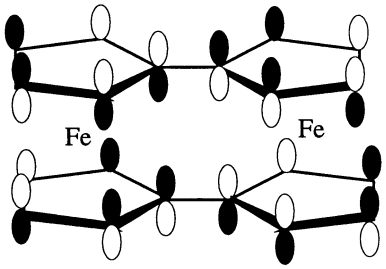

(a)

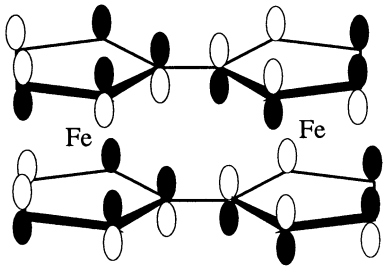

(b)

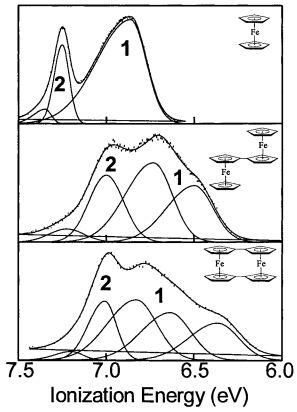

Fig. 5. Close-up spectra of ionization bands **1** and **2** of ferrocene, biferrocene ($Fv(FeCp)_2$), and bis(μ-fulvalenediyl)diiron (Fv_2Fe_2).

4. Discussion

4.1. Comparison to previous studies

The spectroscopic information for these bimetallic fulvalenediyl molecules shows that the general ferrocene electronic structure is for the most part preserved. The assignment of the metal-based ionizations for $Fv(FeCp)_2$ and Fv_2Fe_2 obtained here based solely on experimental information is different from that given by Böhm, who first reported He I photoelectron spectra of these molecules. The only assignment of the metal-based ionizations of these molecules consistent with all the experimental results presented here places the ionizations from the $d_{x^2-y^2}$ and d_{xy} orbitals at lower ionization energy than ionizations from the d_{z^2} orbitals. Böhm assigned the d_{z^2}-based ionizations as the lowest energy ionizations based primarily on calculations performed using the INDO method. The large amount of relaxation and correlation effects encountered in metallocenes has caused the calculation of experimental observables for such molecules to be especially troublesome [40], and interpretation of experimental results for systems like these based upon computational results must be approached with great caution. The assignment given here is the only one consistent with all of the photoelectron spectroscopic results, and also is in agreement with other experimental results for these bimetallic molecules. For example, the EPR spectra of both $[Fv(FeCp)_2]^+$ and $[Fv_2Fe_2]^+$ are consistent with the ground state of the cation as given by our assignment [46].

4.2. Extent of and pathway for electronic communication

The four molecules studied here all show evidence for extensively delocalized π systems in the ligands. As shown for the phenyl-substituted ferrocenes, splittings are observed in the ligand ionization region due to π-interactions between ferrocene ligand-based orbitals and phenyl orbitals. In contrast, no apparent splitting of the metal-based ionizations of the phenyl-substituted ferrocenes are observed, indicating that the broadening of these ionization bands for the bimetallic molecules must be caused by other factors than simple delocalization of the ligand π system or the reduced symmetry of the molecules.

Table 2 lists the overall width of bands **1** and **2**. The width of band **1**, which contains the ionizations from the $d_{x^2-y^2}$ and d_{xy} orbitals of each metal, shows a consistent increase from monometallic to bimetallic molecules and essentially doubles for Fv_2Fe_2 as compared to the monometallic molecules Fig. 5. The width of band **1** increases by 0.22 eV from ferrocene to $Fv(FeCp)_2$, and increases another 0.23 eV from $Fv(FeCp)_2$ to Fv_2Fe_2, indicating a greater degree of metal–metal communication for Fv_2Fe_2 than for $Fv(FeCp)_2$, and suggesting that the extent of broadening is related to the number of bridging fulvalenediyl groups and not to the distance between the metal centers. The ionizations in band **2**, which arise from the d_{z^2} orbitals from each metal, do not show an apparent splitting for either bimetallic molecule. Although the band width of **2** for the bimetallic molecules is somewhat larger than for the monometallic molecules these changes do not show a clear trend and are essentially insignificant because they are only on the order of the width of the narrow vibrational progression associated with ionization from these largely nonbonding orbitals. This also indicates that the minimum-energy molecular geometry for this ion state is not much different from the geometry of the neutral molecule.

As an example to show the importance of both orbital overlap and orbital energy matching for efficient orbital mixing, an energy correlation diagram for FcPh derived from the experimental ionization energies of ferrocene, benzene, and FcPh is shown in Fig. 6. On the left-hand side are the ionization energies of ferrocene. On the right-hand side are the ionization energies of benzene. As shown previously in the results section, the orbitals with bridging carbon character overlap well with each other and form symmetric and anti-symmetric combinations with large splittings as observed for the Cp and CpPh-based ionizations in the 8–10 eV energy region. A close energy matching between the Cp-based orbital

Table 2
Overall widths of bands **1** and **2**

	Band **1**	Band **2**
Ferrocene	0.34	0.11
FcPh	0.37	0.14
$FcPh_2$	0.39	0.14
$Fv(FeCp)_2$	0.56	0.22
Fv_2Fe_2	0.79	0.19

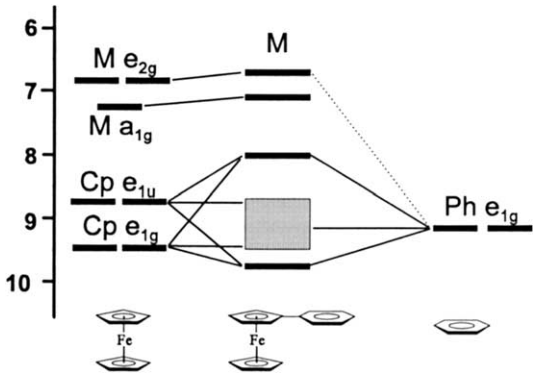

Fig. 6. Energy correlation diagram for phenylferrocene derived from the experimental ionization energies of ferrocene and benzene.

from the ferrocene fragment and the π orbitals of the phenyl fragment contribute to the large splitting of these combinations. The ionizations arising from orbitals with nodes at the bridging carbons do not have good overlap even with close energy matching, and the symmetric and anti-symmetric combinations are not greatly split. Although overlap would be present between one component of the e_{2g}-metal-based orbitals of the ferrocene fragment (due to the ligand character present in this orbital) and the π orbital of the phenyl fragment with bridging carbon character, the energy gap between these two orbitals is much larger and the metal-based ionization band does not show appreciable profile changes from those of ferrocene. A dashed line is used in Fig. 6 to indicate this much weaker interaction that is still allowed by symmetry.

Compared to this example of FcPh, mixing between the metal centers of $Fv(CpFe)_2$ and Fv_2Fe_2 should be favorable because of the close (essentially degenerate) energy matching. But as the experimental results indicate, even with very good energy matching significant orbital mixing is only present between the $d_{x^2-y^2}$ and d_{xy} orbitals of the two metal centers, and is not present for the d_{z^2} orbitals of the two metal centers. In contrast to the broadening observed for band **1** in both bimetallic molecules, the relative sharpness of band **2** indicates that the d_{z^2} orbitals of the two metal centers do not have appreciable communication with each other. This observation is of interest for two reasons. First, the a_{1g} orbital of ferrocene has essentially no ligand character in it. Second, from the results of Penning ionization electron spectroscopic studies of ferrocene [47], it is known that the a_{1g} orbital is as exposed out of the molecule, if not more so, than the e_{2g} orbital. Therefore, any splitting of the metal ionizations from direct metal–metal through-space interactions would be expected to be nearly as pronounced for the d_{z^2}-containing orbitals as for the $d_{x^2-y^2}$ orbitals. The absence of splitting of the d_{z^2}-based orbitals then indicates that through-space interactions are not the major contribution to the strong metal–metal interactions present in these bimetallic molecules.

The atomic character of these orbitals can be visualized by the orbital surface plots of the $d_{x^2-y^2}$ and d_{z^2} orbitals of FcPh (left-hand side) and the combinations of each of these orbitals of Fv_2Fe_2 (right-hand side) from Fenske-Hall calculations shown in Fig. 7. The number below each contour plot is the percentage of total metal character calculated in the orbital. The d_{z^2}-based orbitals for these two molecules each show essentially no ligand density present, while the $d_{x^2-y^2}$-based orbital contains significant electron density from the ligands. The ligand character in this orbital is derived from the empty two-π-node orbitals that have the proper symmetry for back-bonding from the metal d orbitals. Much more ligand character is present in the $d_{x^2-y^2}$-based orbital of Fe_2Fv_2 as compared to FcPh, with the majority of ligand-based electron density residing at the bridging carbons. The greater metal–metal interaction in Fe_2Fv_2 than in $Fv(FeCp)_2$ can be understood because of the presence of two bridging carbon–carbon bonds in Fe_2Fv_2. Fenske-Hall calculations also show that the energy gap between the metal d-orbitals and the empty two-node ligand orbitals is at least 3 eV less for Fv_2Fe_2 than for $Fv(CpFe)_2$. This better energy match results in a stronger interaction in Fv_2Fe_2 than in $Fv(CpFe)_2$, as evidenced by the spreading of band **1** in both bimetallic molecules.

If the amount of contribution to the splitting of band **1** and band **2** from both direct through-space metal–metal and through-ligand metal–metal communication can be separated, the pathway of metal–metal electron delocalization can be better understood. One way in which this can be done is to use a Hückel analysis that utilizes the eigenvalues of and overlap integrals between two metal orbitals from Fenske-Hall calculations to compute the energy splitting using the following for-

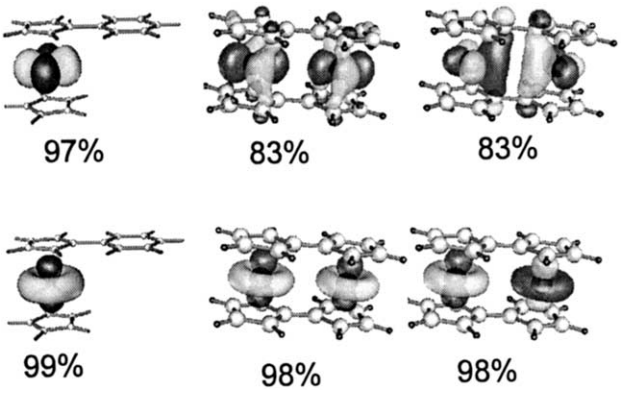

Fig. 7. Orbital surface plots of the metal d_{z^2} and $d_{x^2-y^2}$-based orbitals of FcPh and Fv_2Cp_2 (Fenske-Hall calculations, contour value of 0.028 electrons per $Å^3$), illustrating the greater amount of ligand character in the $d_{x^2-y^2}$-based orbitals of Fv_2Cp_2 and the lack of a direct metal–metal interaction. The number below each contour plot is the percentage of total metal character calculated in the orbital.

mula:

$$\Delta E = E_{\text{antibonding}} - E_{\text{bonding}} = \frac{H_{11} - H_{12}}{1 - S} - \frac{H_{11} + H_{12}}{1 + S}$$

While it is difficult to obtain quantitatively and sometimes qualitatively accurate results with high level calculations for this type of molecule [40], approximate molecular orbital methods such as the Fenske-Hall method are built on the principles of orbital overlap and orbital energy matching, and this method has long been used effectively to reveal the pertinent electronic structure and bonding features of organometallic molecules. In the equation shown H_{11} and H_{12} are the diagonal and off-diagonal energies of the orbitals of interest, and S is the overlap between the two orbitals. The calculated ΔE is then the energy splitting that results only from the direct metal–metal through-space interaction. For Fv_2Fe_2 the overlap integral between the two $d_{x^2-y^2}$ orbitals is 0.00488 and between the two d_{z^2} orbitals is 0.00179, and the ΔE due to through-space interactions is then 0.062 eV for the $d_{x^2-y^2}$ combinations and 0.021 eV for the d_{z^2} combinations. The calculated through-space contributions to the splitting for the $d_{x^2-y^2}$ orbitals are insignificant compared to the spreading observed in the spectra of both Fv_2Fe_2 and $Fv(CpFe)_2$.

Another demonstration is to computationally eliminate the mixing between the metal $d_{x^2-y^2}$ and d_{xy} orbitals of the ferrocene fragments and the empty two-node e_{2g}^*-based orbitals of the Fv ligands. This can be carried out in a Fenske-Hall calculation by deliberately setting to zero the overlap integral between the metal $d_{x^2-y^2}$ and d_{xy} orbitals and empty e_{2g}^*-based ligand orbitals of Fv_2Fe_2. When this is done, the calculated splitting of the metal-based $d_{x^2-y^2}$ combinations changes from 0.77 to 0.03 eV. In another words, of a calculated 0.77 eV splitting, at least 0.74 eV is the result of through-bond interactions between the metal and ligand orbitals and only a maximum of 0.03 eV is from direct through-space metal–metal interaction. Both of these model demonstrations imply that the direct through-space metal–metal interaction in Fv_2Fe_2 is negligible.

4.3. Geometry change upon ionization

Density functional calculations are able to satisfactorily reproduce the geometries of both the neutral and cationic molecules. Selected calculated and experimental bond lengths for Fv_2Fe_2 and $[Fv_2Fe_2]^+$ are listed in Table 3. The calculations agree with our assignment of the photoelectron spectra in that the ground cation state is associated with a state that is ionized from a $d_{x^2-y^2}$-based orbital. The Fe–Fe distance changes from 3.93 to 3.69 Å from the neutral to the ground cationic $^2B_{3u}$ ($d_{x^2-y^2}$) state compared with the experimental values of 3.98 and 3.63 Å. As mentioned previously, this shortening of the experimental distance had been taken to indicate a direct metal–metal interaction. A shortening of the bridging C–C distance by 0.02 Å is also observed. Most significantly, the geometry perturbation that most contributes to the shortened Fe–Fe distance is tilting of the rings in each Fv ligand towards each other. Such tilting is not observed for the higher energy ^2A_g (d_{z^2}), $^2B_{1g}$ (d_{xy}), $^2B_{2u}$ (d_{xy}) cationic states. If the Fv ligands are flattened out but all the other coordinates are kept the same as calculated for the cation state, the Fe–Fe distance changes from 3.69 to 3.88 Å. Fenske-Hall calculations with the geometries from both neutral and cationic $^2B_{3u}$ ($d_{x^2-y^2}$) state show no significant changes of Fe–Fe or Fe–C overlap integrals. The shortened bridging C–C bond length and ligand tilting can be interpreted as being due to the ionization occurring from an orbital with antibonding character at the bridging C–C bond. Both the tilted Fv and shortened bridging C–C bond distance contribute to the shorter Fe–Fe distance in $[Fv_2Fe_2]^+$ species observed in the crystal structure without invoking metal–metal bond formation [17].

Table 3
Experimental and calculated structures of Fv_2Fe_2 and $[Fv_2Fe_2]^+$

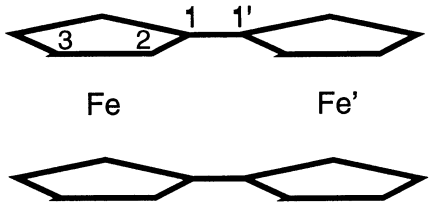

	Fv_2Fe		$[Fv_2Fe_2]+$	
	Obs.	Calc.	Obs.	Calc.
Fe–Fe′ (Å)	3.984(4)	3.928	3.636(1)	3.694
C1–C1′ (Å)	1.476(9)	1.458	1.447(4)	1.443
Fe–C1 (Å)	2.056(6)	2.052	2.085(2)	2.092
Fe–C2 (Å)	2.049(8)	2.044	2.065(2)	2.067
Fe–C3 (Å)	2.054(8)	2.047	2.052(2)	2.068
Angle [a] (°)	178.7	179.8	175.2	175.8

[a] Angle from Cp(centroid)–C1–C1′.

5. Conclusions

The photoelectron spectroscopic study reported here of $Fv(FeCp)_2$ and Fv_2Fe_2 gives a measure of the amount of communication that exists between the two metals as well as an indication of the pathway by which this communication occurs. Good orbital energy matching favors good metal–metal communication, and the appreciable amount of ligand character mixing in the primarily d_{xy}- and $d_{x^2-y^2}$-based orbitals provides a ligand-mediated pathway for metal–metal communica-

tion, which is greater in Fv_2Fe_2 than in $Fv(FeCp)_2$. Any direct through-space metal–metal electron interaction has far less contribution to the ground and excited positive ion states of both Fv_2Fe_2 and $Fv(FeCp)_2$. The communication between the metal centers is greater for Fv_2Fe_2 than for $Fv(FeCp)_2$, but since both bimetallic molecules in their ground ionic states show extensive communication between the two metal centers on the photoelectron spectroscopy timescale, they should both be described as class III species in the gas phase.

Acknowledgements

D.L.L. acknowledges the support by the U.S. Department of Energy (Division of Chemical Science, Office of Basic Energy Sciences, Office of Energy Research, DE-FG03-95ER14574), the National Science Foundation, (Grant No. CHE-9618900), and the Materials Characterization Program, Department of Chemistry, the University of Arizona. HJF would like to thank Julia K. Padden Metzker for providing the ferrocene data and Sandra Rothschild for helpful discussions.

References

[1] S.J. Lippard, J.M. Berg, Principles of Bioinorganic Chemistry, University Science Books, Mill Valley, CA, 1994, pp. 231–254.
[2] D. Astruc, Acc. Chem. Res. 30 (1997) 383.
[3] W. Kaim, A. Klein, M. Glockle, Acc. Chem. Res. 33 (2000) 755.
[4] K.D. Demadis, C.M. Hartshorn, T.J. Meyer, Chem. Rev. 101 (2001) 2655 (and references therein).
[5] C. Creutz, Prog. Inorg. Chem., in: S.J. Lippard (ed.), Wiley, New York, 1983.
[6] M. Brady, W. Weng, Y. Zhou, J. Seyler, A.J. Amaroso, A.M. Arif, M. Bohme, G. Frenking, J.A. Gladysz, J. Am. Chem. Soc. 119 (1997) 775.
[7] S. Barlow, D. O'Hare, Chem. Rev. 97 (1997) 637.
[8] T.T. Chin, R.N. Grimes, W.E. Geiger, Inorg. Chem. 38 (1999) 93.
[9] J. Alverez, Y. Ni, T. Ren, A.E. Kaifer, J. Supramol. Chem. 1 (2001) 7.
[10] P. Nguyen, P. Gomez-Elipe, I. Manners, Chem. Rev. 99 (1999) 1515.
[11] C. Elschenbroich, A. Salzer, Organometallics, A Concise Introduction, 2nd ed., VCH Publishers Inc, New York, NY, USA, 1992, pp. 326–327.
[12] D.O. Cowan, J. Park, M. Barber, P. Swift, Chem. Comm. (1971) 1444.
[13] D.O. Cowan, R.L. Collins, F. Kaufman, J. Phys. Chem. 75 (1971) 2025.
[14] D.O. Cowan, G.A. Candela, F. Kaufman, J. Am. Chem. Soc. 93 (1971) 3889.
[15] F. Kaufman, D.O. Cowan, J. Am. Chem. Soc. 92 (1970) 6198.
[16] R.F. Kirchner, G.H. Loew, U.T. Mueller-Westerhoff, Inorg. Chem. 15 (1976) 2665.
[17] C. Levand, K. Bechgaad, D.O. Cowan, U.T. Mueller-Westerhoff, P. Eilbracht, G.A. Candela, R.L. Collins, J. Am. Chem. Soc. 98 (1976) 3181.
[18] M.B. Robin, P. Day, Adv. Inorg. Chem. Radiochem. 10 (1967) 247.
[19] M. Hillman, A. Kvick, Organometallics 2 (1983) 1780.
[20] M.C. Böhm, R. Gleiter, F. Delgado-Pena, D.O. Cowan, Inorg. Chem. 19 (1980) 1081.
[21] M.C. Bohm, R. Gleiter, F. Delgado-Pena, D.O. Cowan, J. Chem. Phys. 79 (1983) 1154.
[22] M.D. Rausch, J. Am. Chem. Soc. 26 (1960) 1802.
[23] M. Rosenblum, J. Am. Chem. Soc. 81 (1959) 4530.
[24] M. Iyoda, T. Okabe, T. Kondo, S. Sasaki, H. Matsuyama, Y. Kuwatani, M. Katada, Chem. Lett. (1997) 103.
[25] H.-J. Fan, Ph.D. Dissertation, University of Arizona, Tucson, AZ 85721, 1999.
[26] F.-H. Fan, M.D. Carducci, C. Grittini, A. Mendoza, D.L. Lichtenberger, Acta Crystallgr. Sect. C 55 (1999) IU9900154.
[27] D.L. Lichtenberger, G.E. Kellogg, J.G. Kristofzski, D. Page, S. Turner, G. Klinger, J. Lorenzen, Rev. Sci. Instrum. 57 (1986) 2366.
[28] D.L. Lichtenberger, A.S. Copenhaver, J. Electron. Spectrosc. Relat. Phenom. 50 (1990) 335.
[29] ADF 2.3.0, Theoretical Chemistry, Vrije Universiteit, Amsterdam.
[30] E.J. Baerends, D.E. Ellis, P. Ros, Chem. Phys. 2 (1973) 41.
[31] G.T. Velde, E.J. Baerends, J. Comp. Phys. 99 (1992) 84.
[32] C.F. Guerra, J.G. Snijders, G. te Velde, E.J. Baerends, Theor. Chem. Acc. 99 (1998) 391.
[33] M.R. Churchill, J. Wormald, Inorg. Chem. 8 (1969) 1970.
[34] M.B. Hall, R.F. Fenske, Inorg. Chem. 11 (1972) 1978.
[35] B.E. Bursten, J.R. Jensen, R.F. Fenske, J. Chem. Phys. 68 (1978) 3320.
[36] W. Schroeder, K. Martin, B. Lorensen, The Visualization Toolkit, Prentice Hall PTR, Upper Saddle River, New Jersey, 1996.
[37] A.B. Uplinger Diss. Abstr. Int. B, 59-50 (1998) 2197.
[38] J.W. Rabalais, L.O. Werme, T. Bergmark, L. Karlson, M. Hussain, K.J. Siegbahn, Chem. Phys. 57 (1972) 1185.
[39] C. Cauletti, J.C. Green, M.R. Kelly, P. Powell, J. von Tilborg, J. Robbins, J. Smart, J. Electron Spectrosc. Relat. Phenom. 19 (1980) 327.
[40] N.E. Gruhn, D.L. Lichtenberger, Characterization of the Electronic Structure of Transition Metal Carbonyls and Metallocenes, Inorg. Elec. Struct. Spec., vol. 2, 1998.
[41] J.C. Green, Acc. Chem. Res. 27 (1994) 131.
[42] D.N. Hendrickson, Y.S. Sohn, H.B. Gray, Inorg. Chem. 10 (1971) 1559.
[43] J.F. Gallagher, G. Ferguson, S.Z. Ahmed, C. Glidewell, A. Lewis, Acta Crystallogr. Sect. C 53 (1997) 1772.
[44] F.H. Allen, J. Trotter, C.S. Williston, J. Chem. Soc. Sect. A (1970) 907.
[45] D.L. Lichtenberger, N.E. Gruhn, M.E. Rempe, W.E. Geiger, T.T. Chin, Inorg. Chim. Acta 240 (1995) 623.
[46] W.H. Morrison, D.N. Hendrickson, Inorg. Chem. 14 (1975) 2331.
[47] S. Masuda, M. Aoyama, Y. Harada, J. Am. Chem. Soc. 112 (1990) 6445.